designs

MDPI

*Article*

# Assessment of Wind Energy Potential Generated by Vehicles: A Case Study in Mexico

**Luis Alfonso Moreno-Pacheco [1], Leopoldo José Luis Sánchez-Hueto [1], Juan Gabriel Barbosa-Saldaña [1], José Martínez-Trinidad [1], Miguel Toledo-Velázquez [1] and Ricardo Andrés García-León [2,3,*]**

[1] SEPI-ESIME Zacatenco, Instituto Politécnico Nacional, México City 07738, Mexico; lamoreno@ipn.mx (L.A.M.-P.); jbarbosas@ipn.mx (J.G.B.-S.); jomartinezt@ipn.mx (J.M.-T.)
[2] Grupo de Investigación INGAP, Universidad Francisco de Paula Santander Ocaña, Ocaña 546552, Colombia
[3] Programa de ASST, Universidad del Magdalena, Santa Marta 470004, Colombia
* Correspondence: ragarcial@ufpso.edu.co

**Abstract:** This research focuses on analyzing the aerodynamic characteristics of residual air currents generated by vehicle movement and evaluating their feasibility for energy generation, then designing a vertical axis wind turbine. The parameters assessed include the characteristic velocity profile, the average and maximum velocities, disturbance lifetimes, as well as the frequency and probability of recurrence of these disturbances. Using the data, projections are made on the electrical energy amount that can be produced by a wind turbine operating under such wind conditions. Measurements were taken at four locations: three within Mexico City (CDMX) and one on the outskirts. The measurement station, consisting of a 2.35 m vertical tower equipped with eight vertically aligned thermos-resistive anemometers, is installed on medians less than 0.50 m from moving vehicles. The data from within CDMX show maximum wind velocities ranging from 6 to 8 m/s at ground level, while measurements on the outskirts record velocities of up to 19.5 m/s. A probabilistic analysis reveals that usable air currents could be present 58% of the time. Based on electrical production calculations, it is estimated that harnessing this residual energy could power approximately 4500 homes, considering the national cost per kWh and the average electricity consumption of a four-person household.

**Keywords:** anemometry; renewable energy; residual energy; sustainability; wind energy; wind potential

check for updates

**Citation:** Moreno-Pacheco, L.A.; Sánchez-Hueto, L.J.L.; Barbosa-Saldaña, J.G.; Martínez-Trinidad, J.; Toledo-Velázquez, M.; García-León, R.A. Assessment of Wind Energy Potential Generated by Vehicles: A Case Study in Mexico. *Designs* **2024**, *8*, 126. https://doi.org/10.3390/designs8060126

Academic Editor: Yuping He

Received: 19 September 2024
Revised: 7 November 2024
Accepted: 15 November 2024
Published: 26 November 2024

**Copyright:** © 2024 by the authors. Licensee MDPI, Basel, Switzerland. This article is an open access article distributed under the terms and conditions of the Creative Commons Attribution (CC BY) license (https://creativecommons.org/licenses/by/4.0/).

## 1. Introduction

### 1.1. Overview

Currently, the energy requirements of modern society are primarily met by fossil fuels such as coal, oil, and natural gas, which are non-renewable and significantly contribute to air pollution, greenhouse gas emissions, and global warming. The need to become more conscious of energy use while harnessing renewable energy sources highlights the urgent need for countries to review their energy policies and explore renewable energy sources that are free from the drawbacks of fossil fuels and that are environmentally sustainable for future generations.

The transition to renewable energy is crucial and imperative for mitigating climate change and promoting sustainable development. Implementing renewable energy not only reduces carbon emissions but also promotes economic development and job creation in the clean energy sector. The increasing affordability of renewable technologies makes them an attractive option for both industrial and household users. Among different renewable energies, wind energy stands out as a continuous and inexhaustible resource, offering a cost-effective solution and promoting local economic development [1].

The availability of renewable resources (solar radiation, air currents, marine currents, biomass, etc.) makes their implementation feasible in locations where fossil fuels are unavailable or impractical. For instance, electricity generation from wind energy has

been extensively studied, and today, large wind farms harness the energy from natural airflows to produce substantial amounts of electricity [2]. Wind resources are widespread; the Earth itself generates air currents through rotational movements, with heating being caused by solar radiation in the atmosphere, diverse topography, and even human-induced modifications such as urbanization, which promote the creation of air currents.

The advantage idea of the residual air currents associated with the turbulence generated by vehicles traveling on high-velocity roads has been developed recently. In this sense, the idea of taking advantage of the air currents associated with the turbulence generated by vehicles (traffic-induced turbulence—TIT) traveling on high-velocity roads has been developed [3]. The concept is completed by implementing a novel vertical-axis wind turbine (VAWT), which generates electricity by harvesting the aerodynamic turbulent wake resulting from vehicles traveling [4]. The theoretical potential for obtained wind energy from the high-velocity vehicles moving on highways is elevated by considering the traffic roads' milage; in this case, the wind energy can be converted to electricity and connected to the electrical grid. Even in cities where velocity is controlled, the traffic frequency could result in high small-scale energy production to recover energy for sensor systems, street traffic signals, or even street illuminations.

Kumar and collaborators [5,6] showed in a theoretical study that the amount of energy generated by TIT is significant enough to light a road during the night, and the generated amount may depend on the location of the turbine, the vehicle velocity, the distances from the road to the turbine, and others. The authors proposed vertical and horizontal turbines installed in a series at certain distances from each other. Finally, the authors proposed that the energy can be recovered through wind and vibrational energy by tactfully setting up turbines and placing piezoelectric membranes at appropriate sites, creating eco-friendly systems that satisfy energy needs.

Sayais and colleagues proposed the implementation of a modified Savonius vertical-axis wind turbine to use the maximum amount of wind energy generated by vehicles running on highways. In their proposal, the blade is twisted to achieve maximum spin at low pressure in the wind, diminishing the vibration at the gear moment. This implementation also enables the turbine to rotate clockwise and counterclockwise [7]. The height of the blade is 1.09 m, and its width is 0.33 m. The turbine is assembled with a collar, and the blades are fitted with nut bolts; then, to achieve the motion, a 30°-angle curve shape bends the blades, and the turbine shaft is connected to the electric generator. The research also combined the turbine model with a photovoltaic system in case any source fails to provide energy, as another source would keep generating.

Kumar and coworkers [8] utilized experimental studies regarding arrays of VAWTs and placed several in the middle of the Bhopal to Indore highway in India. The VAWTs were built with waste materials like plastic, drums, bicycle rims, etc. The authors tested an array of four rotors and found that the generated electricity can be used for traffic signals, streetlights, and different electronic devices like velocity radars, camera sensors, traffic signals, etc.

An experimental study on the real-time applications of a Sabonius Wind Turbine (SWT) was carried out by Santhankumar and coworkers [9]. The turbine used operated SWTs placed in both the middle of the highways and at the sides of the highways to assess the location where the maximum amount of energy could be harnessed. The authors analyzed four conditions to understand the rotational behavior at different wind velocities. The authors concluded that the middle of the road is the best position for allocating the SWT, and that the monsoons contribute to an increase in 15% of the velocity of the SWT by improving the amount of energy harnessed from wind energy.

Tian and coworkers [10] proposed a VAWT placed on the highway medians, using three-dimensional numerical simulations based on RANS. The authors included different vehicle scenarios, concluding that the VAWT can produce a power of 139.60 W in a six-lane highway, averaging 90–110 km/h in the fast lane.

The feasibility of using VAWT to recover energy from TIT has been proven by several authors [11]. However, the questions about the best VAWT to use and the gap between turbines planted in an array are questions that Tian and collaborators [12] tried to solve in their work. The authors proposed a 3D-CFD transient simulation. In the first part, they compared a Banki rotor, a Savonius rotor, and a Darrieus rotor to find the best VAWT for highway wind energy recovery. In the second part, different arrays were proposed to find the optimal gap for practical applications. Their results indicate that the Darrieus rotor is not suitable for generating energy from the wake of moving vehicles; meanwhile, the Banki rotor is the one that has the best performance in vehicle wake energy recovery, generating an average power of 11.96 W. The Sabonius rotor has similar trends when compared with the Banki rotor, but the closed center in Sabonius presents a stronger block effect of the flow. The results exposed that the rotor provides a maximum power coefficient if the gap is larger (d = 4D) and a maximum normalized power coefficient at a smaller gap (d = 2D).

As can be read in the paragraphs above, harnessing the energy of moving cars is not a new concept. Different works analyze the energy used by vehicles that employ piezoelectric systems [13], and there are works on turbulence and/or air velocities produced by car movement in regard to implementing wind turbines [14–16]. However, designing an efficient wind turbine requires knowledge of wind velocities, flow patterns, and the optimal distances to achieve maximum energy generation without affecting the vehicle safety. Therefore, analyzing wind potential is fundamental for properly developing these systems [17].

### *1.2. Aim of This Work*

This work aimed to investigate the potential for utilizing residual air currents generated by moving vehicles as a sustainable energy source. This study focused on characterizing the aerodynamic properties of these currents in various urban areas within and around Mexico City and assessing their feasibility for wind energy generation. This research aimed to estimate the possible energy savings and economic benefits from harnessing residual wind resources, thereby contributing to the development of roads as active energy-generating infrastructures and advancing the exploration of residual energy sources in urban environments.

On the other hand, this research provides a novel approach to urban wind energy generation by exploring the untapped potential of residual air currents produced by vehicle movement. It offers a comprehensive analysis of the wind velocity profiles and disturbance characteristics of these currents, along with a probabilistic assessment of their availability for energy production. The study's findings contribute to the growing body of knowledge on alternative energy sources, presenting a viable method for integrating wind energy generation into urban infrastructure, which could lead to significant energy savings and promote the sustainability of urban environments.

## 2. Materials and Methods

The methodology applied in this research focuses on collecting anemometric data from the air currents generated by vehicles moving through urban and suburban areas. The experimental procedure is based on real-time simultaneous sampling of air velocities along a vertical line, with a set number of measurement points. This approach is inspired by methods used to characterize air velocity profiles within the discharge section of wind tunnels.

Additionally, national kWh costs and the average electricity consumption of a household with four occupants were considered to estimate that the electrical production from the highway stretch between Mexico City (CDMX) and the city of Santiago Querétaro could power approximately 4500 homes, saving over USD 1,510,174 annually.

### *2.1. Design and Location of the Anemometric Station*

Initially, the main objective was to characterize unconfined and time-varying air currents. The measurement station was equipped with anemometers that operate on the thermal resistance principle (similar to hot-wire anemometers) and simultaneously record wind velocities at eight points distributed along the vertical line. The sampling area (the measurement station is positioned in traffic medians, no more than 0.50 m from the source of the disturbance) covers a total of 1.7 m, starting 0.5 m from ground level, with a sampling frequency of 10 Hz. The structural and performance characteristics of the measurement station allow for instantaneous velocity identification profiles related to the disturbances generated by vehicles in the surrounding air masses.

Furthermore, the tower has a height of 2.35 m, with sensors positioned from the first 0.50 m (measured from the base, which is the height where vehicles typically exhibit a pronounced change in geometry due to bumpers) to almost the tower's full height. The sensors are spaced 0.25 m apart, resulting in 8 anemometers per tower. These dimensions were considered because most vehicles traveling in the high-velocity lane (usually closest to the median, shoulder, or guardrail, areas where wind turbines could potentially be placed) range from small vehicles to large SUVs and pickups. The largest vehicles within these categories have heights slightly exceeding 1.8 m, although the average vehicle height is 1.65 m, while the tower's sampling zone extends to 1.75 m [18].

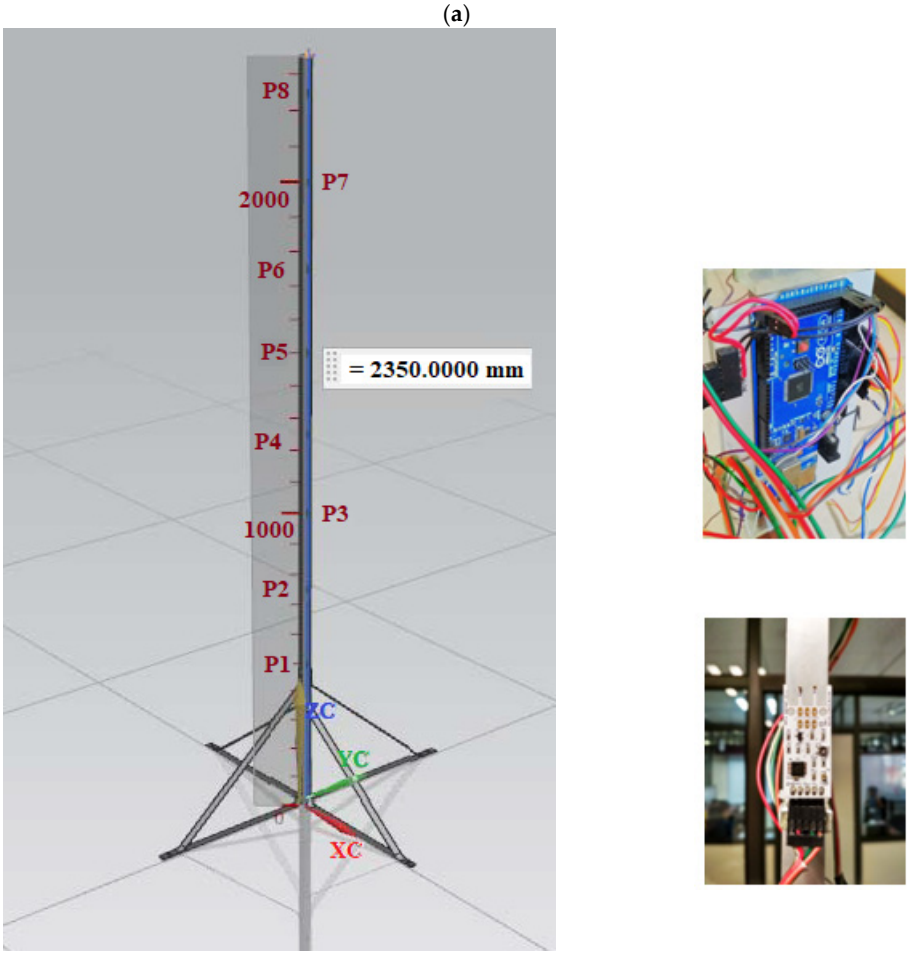
The signals emitted by the sensors are transmitted to an acquisition board (Arduino Mega 2560) and data storage unit, which record the measurements. This information can be instantaneously measured at time intervals controlled by the operator. All sensor readings are oriented in the same direction and aligned along the tube of the measurement station. The anemometers used are MD-0550 sensors, which are sensitive enough to react to light air currents generated from approximately 0.30 m to 0.60 m. One potential application for these sensors includes detecting wind produced by human respiration. The data acquisition and storage system and sensors are powered by a high-discharge 7.4 V, 5000 mAh battery, commonly used in aeromodeling. This configuration eliminates the need for personnel or a computer to log data at the tower's operational site [19].

Sweeping measurement devices obtained velocity profiles within discharge ducts of wind tunnels along a straight path inscribed in the cross-sectional area of the wind tunnel's discharge tube.

Figure 1 shows the locations for the measurements in situ and the data acquisition system built for this research. The measurement locations considered four sites, three within Mexico City and one outside its metropolitan area, as described below: (1) Miguel Bernard St., La Escalera neighborhood, Mexico City, near ESIA Zacatenco, heading southeast. (2) Ribera de San Cosme Av., Santa María la Ribera neighborhood, Mexico City, near San Cosme subway station, heading east. (3) Luis Enrique Erro Av., within the Adolfo López Mateos Polytechnic Campus. (4) At 45 + 800 km, Mexico-Querétaro Highway, heading north (See Supplementary Material S1).




(**a**)




(**b**)

**Figure 1.** (**a**) Measuring device system at different locations and environmental conditions. Own image. Side photographs: Calle Miguel Bernard; central: Av. Ribera de San Cosme. (**b**) Data acquisition system.

### *2.2. Parameters to Evaluate Wind Potential*

#### 2.2.1. Statistical Analysis

The statistical analysis was focused on obtaining representative data such as the overall average wind velocity, the average velocity for each sensor, the maximum recorded wind velocity, certain percentiles, and other metrics that aid in understandingt he residual air current generation phenomenon.

2.2.2. Probabilistic Analysis—Weibull Distribution

The Weibull probability density law is used in wind energy generation projects to model the potential distribution of wind velocity recurrence [20]. The Weibull probability density function for a random variable $\overline{u}$ is as follows:

$$f(\overline{u}, k, \lambda) = \begin{cases} \frac{k}{\lambda}\left(\frac{\overline{u}}{\lambda}\right)^{k-1} e^{-\left(\frac{\overline{u}}{\lambda}\right)^{k}}, & \overline{u} \geq 0 \\ 0, & \overline{u} < 0 \end{cases} \quad (1)$$

where $\lambda$ is the scale factor, closely related to the average wind velocity, and k is the shape factor, which measures the distribution's spread. These factors can be calculated using different methods [21]. One method involves the algebraic manipulation of the Weibull cumulative distribution function. The following equation describes the cumulative frequency of the sample, considering the shape and scale factors:

$$F(t) = 1 - e^{-\left(\frac{t-\delta}{\lambda}\right)^{k}} \quad (2)$$

where F(t) is the cumulative frequency value for the variable t, and $\delta$ is a location parameter within the sample. This factor is often not used and can be considered as zero (for the purposes relevant to the subject at hand, $\delta$ is assumed to be 0, although, for the mathematical breakdown, it will not be omitted). From Equation (2), the following equation is obtained:

$$e^{\left(\frac{t-\delta}{\lambda}\right)^{k}} = \frac{1}{1 - F(t)}$$

We applied the laws of natural logarithms and utilizied the exponential property of logarithms, as demonstrated in Equations (3) and (4):

$$e^{\left(\frac{t-\delta}{\lambda}\right)^{k}} = Ln\left(\frac{1}{1 - F(t)}\right) \quad (3)$$

$$kLn(t - \delta) - kLn(\lambda) = Ln\left[Ln\left(\frac{1}{1 - F(t)}\right)\right] \quad (4)$$

Given the above, it can be approximated by a linear equation $(y = kx - b)$, which can be described as a regression line with the following:

$$y = \ln\left[\ln\left(\tfrac{1}{1-F(t)}\right)\right]; \quad x = \ln(t - \delta); \quad b = k\ln(\lambda)$$

From the last three expressions, it can be concluded that the shape parameter k corresponds to the slope of the regression line. From the expression $b = k\ln(\lambda)$, it is observed that $\lambda$ depends on the intercept b of the regression line and k. Therefore, the following equations were obtained:

$$b = k\ln(\lambda)$$

$$b/k = \ln(\lambda)$$

$$\lambda = e^{\frac{b}{k}}$$

2.2.3. Power Generated by Wind

The theoretical maximum efficiency for a horizontal-axis wind turbine (HAWT) is the Betz limit, which is approximately 0.59. The theoretical analysis for the power generated by VAWT does not follow the Betz limit analysis because the mathematical approach for this

physical scenario is different. Unlike HAWTs, VAWTs can capture wind from any direction. Equation (5) illustrates the computation of $C_p$ for a VAWT system.

$$C_p = \frac{P_M}{P_v} = \left(\frac{2\pi NrF}{60\ s}\right) \Big/ \left(\frac{\rho S {V_v}^3}{2}\right) \quad (5)$$

where $P_M$ = machine power (W), $P_v$ = effective wind power to the area projected by the rotor (W), N = RPM, r = rotor turning radius (m), F = braking force (N), ρ = air density ($kg/m^3$), S = area projected by the rotor ($m^2$), and $V_v$ = wind velocity (m/s).

In environments with rapidly changing wind directions, such as urban zones, it is important to mention that vertical-axis turbines are the best option, as they are best for operating in turbulent environments with low wind velocities. HAWTs are more efficient in electricity production and are more common commercially than VAWTs. However, VAWTs are often found in urban areas due to various advantages, including being quieter and less hazardous due to their lower rotational velocities, and having shorter tower heights, easy installation, and simple maintenance procedures [22–24].

### *2.3. Measurements with Specific Vehicles and Velocities*

In location 3, disturbances generated by three different vehicles (V1, V2, V3), each with distinct dimensions and geometries (considered standard geometries), were measured: (V1) 2005 Pontiac Matiz, (V2) 2008 Ford EcoSport, and (V3) 2013 Chevrolet Malibu. These vehicles were driven around the measurement station at different velocities, ranging from 20 km/h to 100 km/h (with a maximum velocity of 110 km/h for V3), with 10 km/h increments. Each vehicle circled the station at least three times.

Note that the initial measurements can be considered preliminary. Initially, it was necessary to be on-site to tangibly experience the problem and utilize new tools to address it. The measurements taken on Av. Ribera de San Cosme and Miguel Bernard Street provided insights into quantitative patterns in the airflow, thanks to the newly established measurement and maneuvering stations.

The considerations made by these initial measurements were as follows:

- The proximity of the measurement tower to the vehicle traffic: This parameter was constrained by the location of medians or road shoulders, which allowed the measurement tower to be placed no less than 0.5 m from the vehicles.
- Sensors' positions relative to the passing vehicles.
- Uncertainty of vehicle velocities: Initially, vehicle velocities were unknown, making it difficult to make precise inferences about the airflow patterns. A single vehicle produces a specific and somewhat identifiable flow pattern, but the presence of multiple vehicles alters this pattern.
- Large vehicles, such as trucks or buses, create greater disturbances in the air: However, they travel at lower velocities compared to smaller vehicles, which are more prevalent in urban areas.
- Multifactorial nature of disturbance duration: Factors such as velocity, vehicle succession, vehicle dimensions, relative vehicle velocity to natural wind, distance from the measurement station, and environmental conditions, which are not entirely controllable, affect disturbance duration.
- Sensor placement and Arduino card programming: Each sensor had to be positioned in a specific location, or the Arduino card programming had to be adjusted accordingly.

Based on the above considerations and the initial data, graphs like those presented in Figure 2 were generated. The red range represents higher velocities, while the green range represents lower velocities. The red lines in Figure 2a illustrate the chaotic and multidirectional nature of the flow, with purple lines indicating swirling conditions where higher velocities are observed. The subsequent red lines in Figure 2b suggest disturbances within turbulences. Finally, Figure 2c shows the end of a significant and nearly uniform

disturbance and a smooth disturbance from start to finish. Measurements on Miguel Bernard Street yielded the results shown in Figure 2.

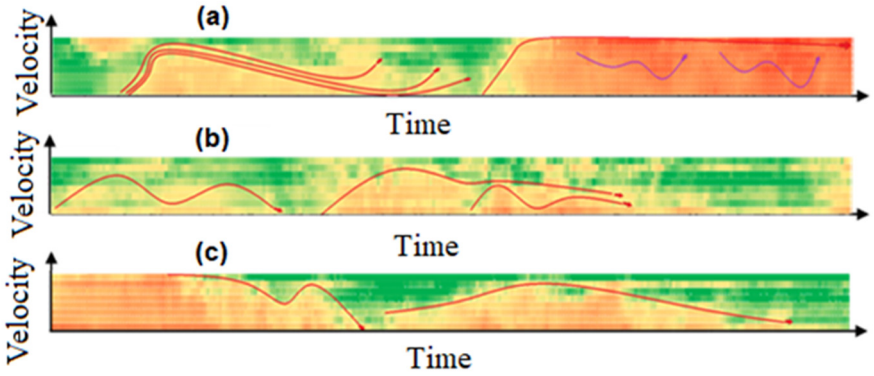



**Figure 2.** Primary velocity fluctuation mapping. (**a**) August 15–14:10 h—Av. Ribera de San Cosme, 24 °C, RH 53%, 1009 hPa—maximum velocity 11.856 m/s—average velocity 2.49 m/s; (**b**) August 16–20:45 h—Av. Ribera de San Cosme, 20 °C, RH 65%, 1008 hPa—maximum velocity 8.977 m/s—average velocity 1.32 m/s; (**c**) August 17–14:00 h—Av. Ribera de San Cosme, 26 °C, RH 49%, 1009 hPa—maximum velocity 7.733 m/s—average velocity 1.91 m/s.

Another qualitative indicator of the presence of a characteristic vertical velocity profile is the consistency observed between the instantaneous profiles recorded during each measurement. As shown in Figure 3, higher velocities are predominant in position two [25]. Each profile column represents the profile's evolution across ten samples (from top to bottom), representing a randomly selected sample (although the profiles on the left were recorded before those on the right).

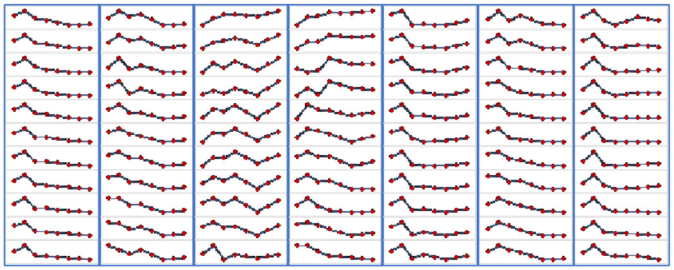


**Figure 3.** Velocity profiles taken randomly from the sampling carried out on the CDMX-QRO highway. Measurement of the median strip on the side adjacent to the high-velocity lane.

Finally, this profile pattern indicates the trend and describes nearly all aerodynamic conditions during the sampling. Based on these results, it was decided to calculate the overall average velocity of the complete sample, $\overline{V}_{pg}$ (general average velocity), as well as the average velocities recorded at each sensor position, $\overline{V}_{pn}$ (average velocity at position "n"), where "n" refers to the sensor position, where n = 1 corresponds to the sensor located 0.50 m above the ground, and n = 2 corresponds to the sensor positioned 0.75 m above the ground, continuing the sequence until covering all sensors and thus the entire sampling length.

The value of $\overline{V}_{pg}$ for the sample was 5.375 m/s. Each sampling position had the values summarized in Table 1. These average velocities, $\overline{V}_{pg}$ and $\overline{V}_{pn}$ (with n = [1–8]), were used to calculate a diameter ratio for the structural design of the wind turbine rotor.

**Table 1.** Average velocities ($\overline{V}_n$) at each position of the measuring station.

| Position | | | | | | | |
|---|---|---|---|---|---|---|---|
| 1 | 2 | 3 | 4 | 5 | 6 | 7 | 8 |
| 6.3406 | 7.5281 | 5.5824 | 4.5997 | 4.6660 | 4.7354 | 4.7617 | 4.7881 |
| $\xi_n$ = radial proportion—$\overline{V}_n/\overline{V}_g$—[$\overline{V}_g$ = 5.375 m/s] | | | | | | | |
| 1.1796 | 1.4005 | 1.0385 | 0.8557 | 0.8681 | 0.8810 | 0.8859 | 0.8908 |

### *2.4. Wind Turbine Design*

The wind turbine design was conducted using Siemens NX, a sophisticated computer-aided design (CAD) software known for its advanced modeling capabilities. The following methodology outlines the steps to develop the wind turbine design, from initial concept to detailed drawing.

(1) Initial Concept and Requirements Analysis: The design process began with thoroughly analyzing the wind turbine's operational requirements, including expected wind velocities, environmental conditions, and performance specifications. This analysis informed the design parameters and constraints, ensuring the final model met the necessary functional and structural criteria.

(2) Preliminary Design and Sketching: Using Siemens NX, preliminary sketches of the wind turbine were created to visualize the basic design concepts. This step involved creating basic shapes. We utilized NX's sketching tools to draft fundamental geometric shapes that represent the main components of the wind turbine, such as the rotor blades, hub, and tower. Defining Dimensions: Applying dimensions to the sketches to establish the scale and proportions of each component based on the analysis conducted in the initial phase.

(3) Three-Dimensional Modeling: Once the preliminary sketches were approved, the 3D modeling process commenced: Creating 3D Components: Transforming the 2D sketches into 3D models using NX's solid modeling tools. This included extruding, revolving, and lofting operations from the rotor blades, hub, and tower. Assembly Modeling: Assembling the individual 3D components into a complete wind turbine model. NX's assembly tools were used to position and align components accurately, ensuring proper fit and function.

(4) Design Optimization: To enhance the performance and efficiency of the wind turbine, design optimization was performed: Finite Element Analysis (FEA): Conducting stress and strain analysis using NX's FEA module to evaluate the structural integrity of the wind turbine components under various loading conditions. Aerodynamic Testing: Simulating airflow around the turbine using NX's aerodynamic analysis tools to optimize blade shape and improve energy capture efficiency.

(5) Detailed Drawings and Documentation: The final step involved generating detailed technical drawings and documentation: Creating Detailed Drawings: Utilizing NX's drafting tools to produce comprehensive technical drawings of each component and assembly, including dimensions, materials, and manufacturing notes. Documentation: Preparing design documentation that includes specifications, assembly instructions, and maintenance guidelines to support the manufacturing and installation processes.

(6) Review and Iteration: The completed design was reviewed and iterated based on feedback and testing results. Adjustments were made to refine the design and address any identified issues, ensuring the final product meets all performance and safety requirements.

## 3. Results and Discussions

### *3.1. Statistical Analysis*

Although the measurements taken at locations A and B showed average wind velocities between 2.5 m/s and 3.5 m/s, with maximum velocities ranging between 6 m/s and

8 m/s, they are not considered optimal for applying a wind generation project. However, it provided valuable insights that frame and explain the nature and complexity of the measurements and the problem in greater depth. The following observations emerged from these initial measurements:

- Sensor arrangement relative to the Arduino programming: Each sensor must be placed in a specific position, or the programming on the Arduino board needs to be modified to assign a different location. This behavior is due to sensor malfunctions or the need for replacements. Each sensor follows a specific calibration curve and cannot be interchanged with others.
- Orientation of the measurement readings: Defining the orientation of the measurements about vehicle movement is essential as this affects the accuracy of the collected data.
- Positioning and proximity of the measurement tower: The tower's placement is dependent on the road infrastructure, such as medians, barriers, and lane dividers. The minimum distance that the measurement station can be positioned near vehicles is no less than 50 cm.
- Variations in vehicle airflow: Although vehicles have velocity limits at the study locations, airflow variations are influenced by several factors.
- Time intervals between vehicles and other factors: The time gaps between vehicles, their different geometries, travel velocities, and the interaction of these factors create a wide range of airflow conditions.
- Vehicle velocity modifications: Vehicle velocities are affected by traffic lights, road accidents, pedestrian interactions, traffic congestion, etc.
- Variability in airflow disturbances: This factor influences the lifespan and continuity of airflow disturbances.
- Sensitivity of wind turbines: A wind turbine is sensitive to the air currents resulting from the interaction between vehicle-generated flows and natural wind currents.
- Further research into urban wind potential: There is a need to delve deeper into the wind energy potential within cities and urban areas.

#### 3.1.1. Flow Patterns Identified, Measurements at Location 3

Figure 4 shows the graphs of the flow patterns identified as "pulsating flows" detected from measurements at Location C. These curves correspond to vehicle velocities ranging from 20 km/h to 60 km/h. The results differ from each other based on the visualized pattern geometry and the characteristics of the observed airflow. It is important to keep the vehicle geometries in mind: V1 is a compact vehicle with a rounded geometry, V2 is an SUV-type vehicle with a robust, square, and angular geometry, and lastly, V3 is a sedan with a streamlined geometry and smooth edges.

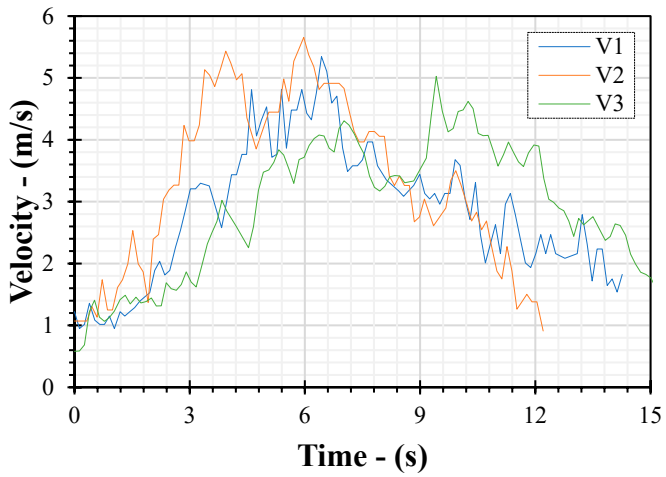



**Figure 4.** Visualization of pulsating flow patterns.

Figure 5 shows the flow curve patterns identified as "pulsating flows followed by a wake", corresponding to vehicle velocities between 70 km/h and 90 km/h (the same for Figure 6). The highest-magnitude velocities are obtained from the disturbances generated by V2, although these can also be considered the most chaotic. It is evident that, in all cases related to this second type of disturbance, the disturbance lifespan increases considerably, as does the magnitude of the maximum velocity recorded for vehicles V2 and V3, ranging from 5.5 m/s to 6.5 m/s and from 5 m/s to 6 m/s, respectively, as mentioned in reference [26].

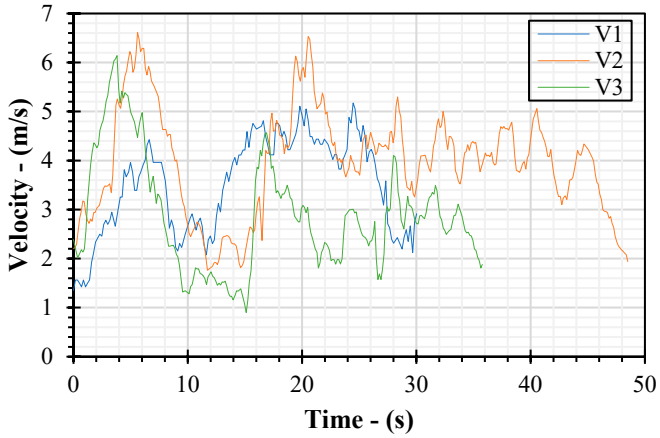



**Figure 5.** Visualization of pulsating wake-type flow patterns.

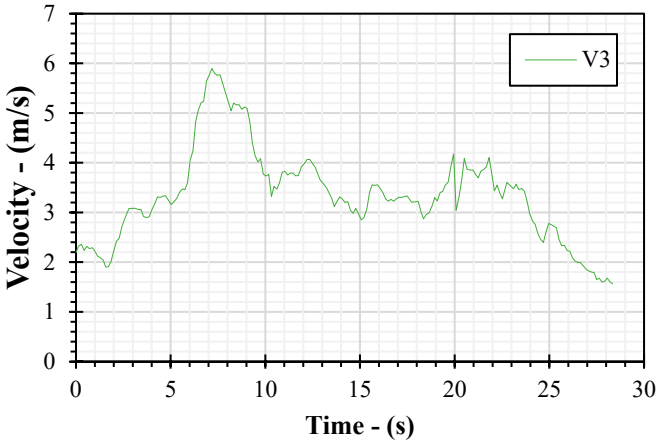



**Figure 6.** Visualization of intense pulsating flow patterns, without apparent wake.

Figure 6 presents a pulsating disturbance, and only V3 was subjected to this type of test since the infrastructure used in this experiment did not allow V1 or V2 to reach high velocities. It cannot be confirmed that the flow is followed by a wake, or at least not a well-defined one. It may be a pulsating flow, now much stronger than that generated at lower velocities, which, during the dissipation process, encounters a faint wake, thus "hiding" within the pulse; or the geometry of the vehicle might allow it to "cut through the air" without significantly disturbing it.

### 3.1.2. Sampling at Location 4

Table 2 shows the value $\overline{V}_g$ (average velocity), which was 5.375 m/s. The velocities $\overline{V}_g$ and $\overline{V}_n$ (average velocity for each measurement point "n"), with n = [1–8], were later used to calculate a radial velocity ratio ($\xi_n$) to obtain the standard or dimensionless geometry of the velocity profile. The maximum velocity recorded during the experiment was 19.514 m/s, registered at position 2 of the measurement station. The 10th percentile (p10) is 2.577 m/s, the p50 is 5.134 m/s, the p75 is 6.73 m/s, and the p95 is 9.745 m/s.

**Table 2.** Average velocities at each measuring station position.

| Power (W) | Power per km (W) | Production Bi-Monthly per km (kWh) | Savings Bi-Monthly per km (USD) | Savings Annual per km (USD) | Savings Annual per 100 km (USD) |
|---|---|---|---|---|---|
| 50 | 16,666 | 12,060.65 | 1.67 | 10.05 | 1005.70 |
| 60 | 20,000 | 14,472.79 | 2.01 | 12.08 | 1208.46 |
| 70 | 23,333 | 16,884.92 | 2.35 | 14.11 | 1411.22 |
| 80 | 26,666 | 19,297.05 | 2.70 | 16.13 | 1614.00 |
| 90 | 30,000 | 21,709.18 | 3.02 | 18.16 | 1817.75 |
| 100 | 33,333 | 24,121.31 | 3.36 | 20.19 | 2019.51 |
| 110 | 36,666 | 26,533.44 | 3.70 | 22.22 | 2222.28 |

The velocity profile obtained corresponds to the entire length of the sampling section. It can be observed in Figure 7 that at measurement point 2, there is an increase in wind velocity; starting from position 3 and onwards, there are decreases in wind velocity to the extent that, over the total sampling length, lower velocities than $\overline{V}_{pg}$ are recorded in the upper part of the profile. This behavior is contrasted with what a straight-blade Savonius rotor (dotted line in Figure 7) would experience. It is understood that these machines assume a uniform flow in terms of velocity gradients (or that they could capture both upper and lower flows), and therefore, the rotor can harness the total incoming flow. However, the measurements indicate that the profile is not constant but shows significant variations for this specific case of wind generated by vehicles.

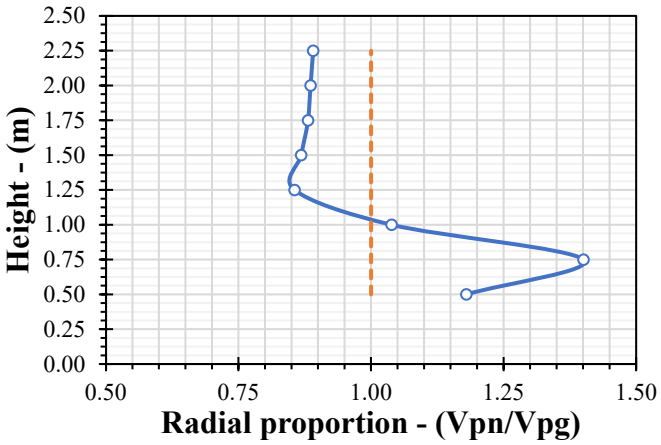



**Figure 7.** Velocity profile referring to the measurement section considering the actual positions of the measurement points (1.75 m).

Furthermore, Table 1 considers the use of currents produced in a single direction of vehicular flow, the placement of ~333 rotors (which can be placed in counter-rotation to avoid blocking effects) per kilometer of roadway, and the assumption that only 70% of the road has straight sections where high velocities can be achieved.

### *3.2. Weibull Distribution and Energy Economic Savings*

Based on the measurements taken on the Mexico–Querétaro highway, the relative frequency graph in Figure 8 identifies a wind velocity range crucial for the efficient and safe operation of the machine. The graph analysis aims to establish an optimal operational range where the machine can perform consistently without compromising its structural integrity. Excessively high rotational velocities could damage the rotor and pose safety risks. Savonius rotors generally require wind velocities between 1.5 m/s and 3 m/s to

overcome static inertia [24]. The relative frequency graph indicates that the most common wind velocity is around 5.0 m/s, while the Weibull distribution trend line predicts a slightly lower peak velocity of 4.5 m/s over time. Both values are close to the calculated average velocity of 5.38 m/s, suggesting that setting the operational velocity at 5.0 m/s aligns well with the average velocity range of 4.5 to 5.38 m/s, which would ensure the machine operates efficiently at least 50% of the time without risking its durability.

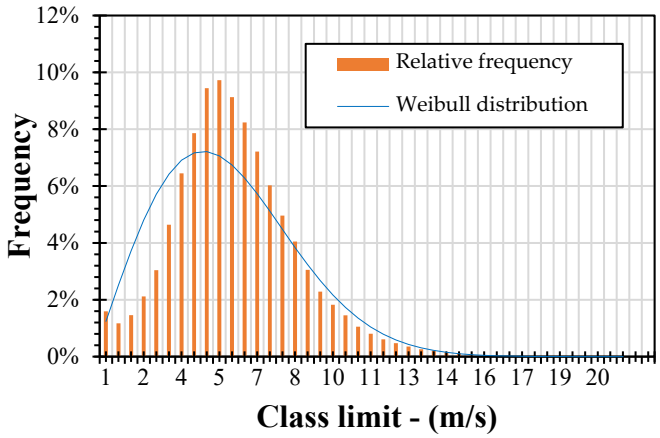



**Figure 8.** Relative frequency distribution with a splice of Weibull frequency distribution plot.

A startup velocity of at least 2.0 m/s and a maximum operational wind velocity of 10.5 m/s were assumed, and the Weibull distribution indicates that the machine could operate approximately 85% of the time, providing over 20 h of daily electricity production. The graph further confirms that the most frequent wind velocity is 5.0 m/s, closely matching the Weibull trend's predicted velocity of 4.5 m/s. This consistency indicates that the machine can reliably and safely generate electrical energy for most of the time, even with the influence of disturbances caused by passing vehicles.

Figure 9 shows a power projection that an aerogenerator could develop, considering a wind velocity of 8.4 m/s (which is 80% of the previously considered maximum operational velocity) and an air density of 1.207 kg/m$^3$ (equivalent to the air density in Mexico City) [27]. This information generates power curves to evaluate unknown parameters (S and $C_p$) that can be substituted into Equation (4).

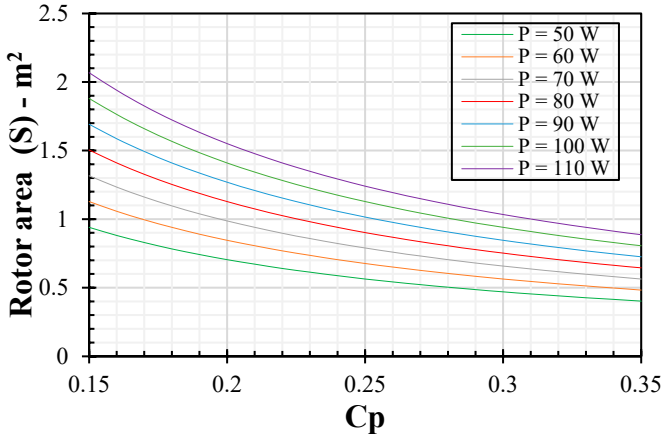



**Figure 9.** Power curves developed considering a vertical axis wind turbine.

Table 2 presents the potential energy production and monetary savings that could be generated based on different production capacities. In preparing this table, it was considered that there would be a 3 m separation between each machine. The total operational probability proposed (85% according to the Weibull distribution) was also considered, as

well as the consistency with the samples taken (99%) where the same roadway section was analyzed, and the minimum daily vehicle traffic consistency, which aligns with the times of the measurements conducted in this experiment (58.9%) [28]. Regarding monetary savings, the price of kWh in Mexico was considered: the first 75 kWh consumed costs USD 0.040, the next 65 kWh costs USD 0.05, and any additional kWh costs USD 0.15. More details for the economic analysis included the build costs of the HVAWT, for this prototype experiment was unique and needed the implementation of a sensor to measure different variables.

Considering the above, it is estimated that there is a relationship between the geometric characteristics of vehicles and the velocity contour geometries. In all cases, the disturbances generated by V2 exhibit a more chaotic nature compared to those from V1 or V3. Additionally, at velocities above 60 or 70 km/h (depending on the vehicle's characteristics), the flow pattern completely changes and seems to split into a pulsating flow and a wake. With this flow pattern, the pulse could be used to overcome the static inertia of the wind turbine, while the wake could provide continuous movement. For velocities exceeding 100 km/h, it is necessary to delve deeper into the analysis of flows to characterize them fully.

Although there was traffic at the last location (D) comprising vehicles of all sizes, a trend shows that higher velocities are recorded at the bottom of the profile. This does not mean that larger vehicles do not generate air disturbances (which could tentatively be greater), but rather that positioning the station next to the median (which is beside the high-velocity lane) records the velocities of vehicles that can travel faster while heavy trucks or cargo vehicles are located in the central or slower lanes away from the median.

The energy developed by these machines could be used to power lighting and/or communication systems. However, considering a household that consumes 400 kWh every two months, each kilometer of roadway with 80 W wind turbines could supply energy to 48 houses or power energy supply systems such as gas stations or electric vehicle charging stations. A continuous power supply system for electric vehicles through magnetic induction is also possible.

Based on the power output of 80 W per wind turbine, the investment cost for each machine is out of reach of this investigation. The turbines could be made from recycled plastics since the only requirement is that they can withstand the local climate conditions, and plastic can meet these needs, reduce production costs, and promote recycling [8]. Mexico has more than 350,000 km of roadways, of which 15,252 km are structurally compatible with the measurement locations.

### *3.3. Construction of the Wind Turbine*

Figure 10 shows the helical-blade Savonius-type rotor used to construct the wind turbine. Note that a helical-blade Savonius-type rotor is a variation on a traditional Savonius wind turbine rotor, distinguished by its helical or spiral blade design. Unlike the classic Savonius rotor, which features vertical or semi-vertical scoops, the helical-blade version incorporates blades that twist around the rotor's axis in a helical manner.

The underlying principle for modifying a helical-blade Savonius rotor is that it will exhibit improved dynamic performance due to the more consistent torque coefficients throughout the entire rotation of the blades (where the moment coefficient always remains positive), ensuring smooth rotational motion. The mechanical stresses caused by drag effects transmitted to the shaft and blades are less aggressive. The literature review has also indicated that these machines exhibit better power coefficients than their simpler counterparts with straight blades.

The final rotor is designed with geometric characteristics that offer optimal functionality for Savonius rotors, including the following features: helical blades, a central recirculation hole, absence of a central shaft or support, a maximum of three blades, and upper and lower plates.

An increase in the operational life of the generated flows will ensure that a wind turbine remains in operation until a new disturbance occurs in the environment, either

from another vehicle or from natural air currents. Therefore, the characterized velocity profile shows a "reduction" in the magnitude of the velocities. This reduction may be due to the geometric vehicle characteristics, as the vehicle does not impact the air mass uniformly; instead, the bumper area initially makes the impact.

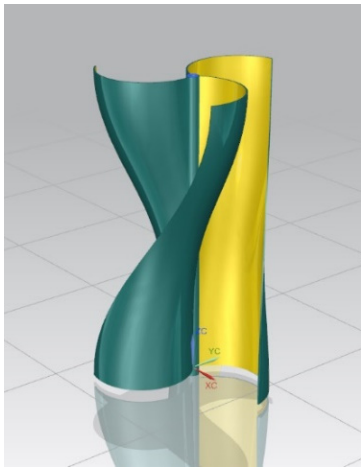


**Figure 10.** Helical Savonius rotor model.

#### 3.3.1. Shape of Rotor Blades

The plates that make up the rotor blades maintain the shape of the vertical velocity profile, considering the respective helical twist of each blade. The process for shaping the blades can be outlined as follows:

(1) Imagine a straight plate with rectangular dimensions.
(2) Overlay the found velocity profile onto the rectangular plate, making the necessary modifications to the blade surface.
(3) "Rotate" the modified blades with the respective twist or helical torque angle.

This process is illustrated in Figure 11, which represents the preliminary approximations of what the rotor of the machine would look like. Specific measurements, geometries, or relationships are not considered (only illustrative).

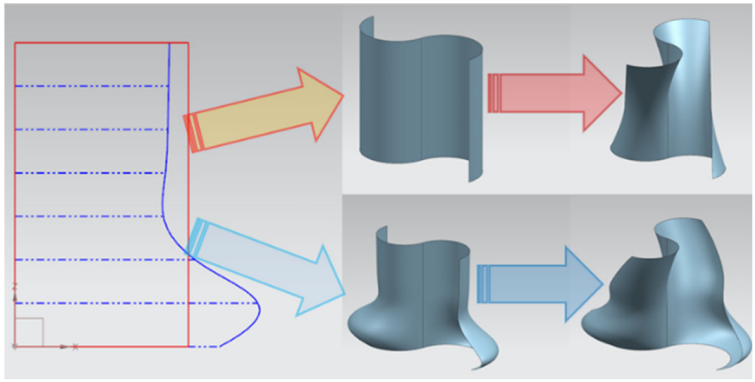


**Figure 11.** Process of visualization of modification of a Savonius helical rotor.

#### 3.3.2. Rotor Sizing

The treatment for sizing the rotor is based on aerodynamic profile considerations and information from the literature.

Field measurements reveal a section of the profile where strong perturbations occur, with wind velocities reaching nearly 140% of the average recorded velocity. These readings develop between measurement points 1 and 3 (the first 50 cm of the sampling length), with

the highest velocities recorded at point 2. From measurement points 3 to 8, wind velocities are below average, ranging between 85% and 99% of the average (see Table 1).

Following these observations, the following considerations were made: (1) the machine should not be excessively large given its intended application; (2) starting from measurement point 4, $\overline{V}_{pn}$ varies insignificantly for each sensor, and thus $P_{rn}$ shows the same trend. Consequently, the height of the machine will be restricted to 1.0 m, and from 75 cm in height, $P_r$ is constrained to a value of 0.8557.

The next value to define is AR; the aspect ratio is a geometric factor characteristic of the rotor. However, due to the design process commonly used for Savonius machines in both variants (straight blades or helical blades), there is no consistency in a specific value in the research. The literature shows values ranging from 0.5 to 6, often depending on the infrastructure and resources available to the researcher or the type of test conducted (a large percentage of experiments are carried out in wind tunnels, either with modifications in the discharge area or a test subject to confinement in the testing section). For this experiment, the AR value will be 1.5.

Considering the central recirculation space, the geometric shape of the velocity profile transport and diameters for each measurement station must be calculated. Kamoji et al. (2009) determined that the presence of a central support shaft reduces the rotor's mechanical performance. Therefore, it is proposed that the rotor has a central recirculation space with a diameter corresponding to 10% of the rotor diameter [24]. Additionally, the rotor diameter for each measurement station is influenced by H, AR, and $P_{rn}$ variables; the factors' product results in the rotor diameter for each measurement point $\varnothing_{rn}$. Table 3 shows the diameter values corresponding to each measurement position.

**Table 3.** Rotor assembly process for each measuring position.

| Variable | Position | | | | |
|---|---|---|---|---|---|
| | **1** | **2** | **3** | **4** | **5** |
| $\overline{V}_{pn}$—m/s | 6.3406 | 7.5281 | 5.5824 | 4.5997 | 4.6660 |
| $P_{rn}$ | 1.1796 | 1.4005 | 1.0385 | 0.8557 | 0.8557 |
| $\varnothing_{rn}$—mm | 786.3956 | 933.6780 | 692.3599 | 570.4742 | 570.4742 |
| $e_n$—mm | 78.6396 | 93.3678 | 69.2360 | 57.0474 | 57.0474 |
| $\varnothing_{pn}$—mm | 432.5176 | 513.5229 | 380.7979 | 313.7608 | 313.7608 |

The variation in the diameter of the recirculation hole across the entire rotor can be observed. In the rotor design and prototype construction, all diameters are standardized by averaging them, resulting in a value of 71.06 mm. Note that 800 mm and 600 mm diameters are considered for the top and bottom plates, respectively (See Supplementary Material S2).

With the established dimensions, a CAD model of the rotor was created using SIEMENS NX software. Two models were developed: one with two blades, and another with three blades. In both cases, complementary twist angles are used (the aim is to ensure that wind always impacts a concave area of a blade; this assumption is achieved by restricting the twist angle so that the product of the angle and the number of blades results in at least 180°). The twist angle for the two-blade rotor is 90°, and for the three-blade rotor, it is 60°. Figure 12 illustrates the different designs; the top part shows the two-blade rotor and the bottom part shows the three-blade rotor [28–31].

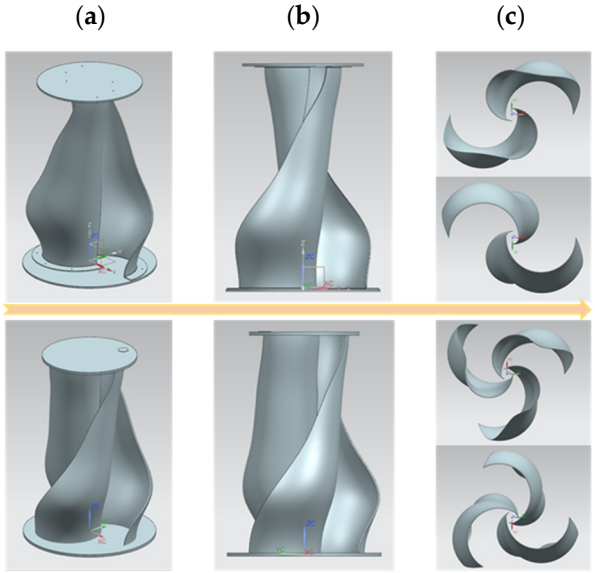



**Figure 12.** Representation of the modified 2- and 3-blade rotors. (**a**) Isometric view, (**b**) lateral view, and (**c**) top and bottom views.

## 4. Conclusions

The measurements taken on August 15, 16, and 17 at Av. Ribera de San Cosme reveal notable variability in recorded wind velocities, ranging from average velocities of 1.32 m/s to 2.49 m/s, with peak velocities reaching 11.856 m/s. While these measurements provide insights into the complex nature of airflows generated by moving vehicles, they also indicate that the conditions may not be ideal for immediate application in wind power projects due to the instability and variability of the recorded velocities.

The observed flow patterns at the study locations show significant variability in disturbances caused by vehicles. These disturbances are influenced by factors such as vehicle geometry, velocity, and road conditions. Notably, pulsating flows and wakes can increase wind velocities substantially, though this increase is uneven.

Analysis of average velocities and radial proportions at location 4 identified a distinct velocity profile for the sampling area, showing an increase in wind velocity closer to the ground and a subsequent decrease with greater sensor height. This variation underscores the challenge of maintaining a consistent and uniform flow—an essential factor for designing efficient wind power systems.

The examination of Weibull distribution and the subsequent energy economic savings analysis suggests that, while the average operating velocities are within a suitable range for activating Savonius-type wind turbines, the feasibility of these systems in urban environments depends on the frequency and stability of the vehicular disturbances. It is anticipated that a wind power system could operate effectively approximately 85% of the time under these conditions, offering substantial energy savings if deployed on a larger scale.

Using Siemens NX in the design process was instrumental in developing a robust and efficient wind turbine model. The software's advanced features in sketching, 3D modeling, optimization, and documentation facilitated the creation of a design that meets operational and performance specifications.

Overall, the findings highlight the need for further research into wind potential in urban settings, focusing on overcoming current limitations and exploring turbine design and placement improvements to enhance efficiency and minimize costs.

**Supplementary Materials:** The following supporting information can be downloaded at: https://www.mdpi.com/article/10.3390/designs8060126/s1, Supplementary Materials S1 and S2.

**Author Contributions:** Conceptualization, L.A.M.-P., L.J.L.S.-H., J.G.B.-S., J.M.-T., M.T.-V. and R.A.G.-L.; methodology, L.A.M.-P., L.J.L.S.-H., J.G.B.-S., J.M.-T. and M.T.-V.; software, L.A.M.-P. and L.J.L.S.-H.; validation, L.A.M.-P., L.J.L.S.-H., J.G.B.-S., J.M.-T. and M.T.-V.; formal analysis, L.A.M.-P., L.J.L.S.-H. and R.A.G.-L.; writing—original draft preparation, L.A.M.-P. and L.J.L.S.-H.; writing—review and editing, R.A.G.-L.;All authors have read and agreed to the published version of the manuscript.

**Funding:** This work was completed in the LABINTHAP of the IPN, supported by the research grants 20241361 and 20232797 of the Instituto Politécnico Nacional of Mexico.

**Data Availability Statement:** The original contributions presented in this study are included in the article/Supplementary Materials. Further inquiries can be directed to the corresponding author(s).

**Acknowledgments:** Thanks go to the Instituto Politécnico Nacional—ESIME Zacatenco, and the National Council of Science and Technology (CONACYT) for all the support given for this research. Also, thanks go to NUMECA International for the software provided for this project.

**Conflicts of Interest:** The authors declare that they have no known competing financial interests or personal relationships that could have appeared to influence the work reported in this paper.

## Abbreviations and Nomenclature List

| | |
|---|---|
| $r_r$ | Root radius |
| $r_t$ | Tip radius |
| $r_m$ | Mean radius |
| h | Height |
| R | Gas constant |
| $\dot{m}_3$ | Compressor delivery air mass flow |
| $T_{t3}$ | Compressor delivery temperature |
| $P_{t3}$ | Compressor delivery pressure |
| $\Delta P_{3-4}/q_{ref}$ | Pressure loss factor |
| $\Delta P_{3-4}/P_{t3}$ | Total pressure loss in the combustor |
| mc | Number of carbon atoms in the fuel |
| mh | Number of hydrogen atoms in the fuel |
| ms | Number of sulfur atoms in the fuel |
| $\%\Delta P_{sf}$ | Pressure loss in the secondary flow, approximately 4% |

## References

1. Petersen, E.L. In search of the wind energy potential. *J. Renew. Sustain. Energy* **2017**, *9*, 52301. [CrossRef]
2. Lonca, G.; Muggéo, R.; Imbeault-Tétreault, H.; Bernard, S.; Margni, M. Does material circularity rhyme with environmental efficiency? Case studies on used tires. *J. Clean. Prod.* **2018**, *183*, 424–435. [CrossRef]
3. Kalthoff, N.; Bäumer, D.; Corsmeier, U.; Kohler, M.; Vogel, B. Vehicle-induced turbulence near a motorway. *Atmos. Environ.* **2005**, *39*, 5737–5749. [CrossRef]
4. Saqr, K.M.; Musa, M.N. A perspective of the Malaysian highway energy consumption and future power supply. *Energy Policy* **2011**, *39*, 3873–3877. [CrossRef]
5. Kumar, M.; Kumar, K.; Rana, R. Wind energy generation from traffic movement. *DU J. Undergrad. Res. Innov.* **2016**, *2*, 116–120.
6. Kumar, M.; Kumar, K. Traffic-Driven energy generator. *Technol. Lett.* **2016**, *3*, 10–13.
7. Sayais, S.Y.; Salunkhe, G.P.; Patil, P.G.; Khatik, M.F. Power generation on highways by using vertical axis wind turbine & solar system. *Int. Res. J. Eng. Technol.* **2018**, *5*, 2133–2137.
8. Kumar-Rathore, M.; Agrawal, M.; Baredar, P. Energy production potencial from wake of moving traffic vehicles on a highway by the array of low economic VAWT. *Mater. Today Proc.* **2021**, *46*, 5272–5277. [CrossRef]
9. Santhakumar, S.; Palanivel, I.; Venkatasubramanian, K. A study on the rotational behaviour of a Savonius wind turbine in low rise highways during different monsoons. *Energy Sustain. Dev.* **2017**, *40*, 1–10. [CrossRef]
10. Tian, W.; Mao, Z.; An, X.; Zhang, B.; Wen, H. Numerical study of energy recovery from wakes of moving vehicles on highways by using a vertical axis wind turbine. *Energy* **2017**, *141*, 715–728. [CrossRef]
11. Kurz, D.; Bugala, A.; Gluchy, D.; Kasprzyk, L.; Szymenderski, J.; Tomczewski, A.; Trzmiel, G. The use of renewable energy sources in road construction and public transport: A review. *Energies* **2024**, *17*, 2141. [CrossRef]
12. Tian, W.; Song, B.; Mao, Z. Numerical investigation of wind turbines and turbine arrays on highways. *Renew. Energy* **2020**, *147*, 384–398. [CrossRef]
13. İlkiliç, C. Wind energy and assessment of wind energy potential in Turkey. *Renew. Sustain. Energy Rev.* **2012**, *16*, 1165–1173. [CrossRef]

14. Keyhani, A.; Ghasemi-Varnamkhasti, M.; Khanali, M.; Abbaszadeh, R. An assessment of wind energy potential as a power generation source in the capital of Iran, Tehran. *Energy* **2010**, *35*, 188–201. [CrossRef]
15. Wu, J.; Wang, J.; Chi, D. Wind energy potential assessment for the site of Inner Mongolia in China. *Renew. Sustain. Energy Rev.* **2013**, *21*, 215–228. [CrossRef]
16. Alayat, M.M.; Kassem, Y.; Çamur, H. Assessment of Wind Energy Potential as a Power Generation Source: A Case Study of Eight Selected Locations in Northern Cyprus. *Energies* **2018**, *11*, 2697. [CrossRef]
17. Morbiato, T.; Borri, C.; Vitaliani, R. Wind energy harvesting rom transport systems: A resource estimation assesment. *Appl. Energy* **2014**, *133*, 152–168. [CrossRef]
18. García-León, R.A.; Gomez-Camperos, J.; Jaramillo, H. Bibliometric analysis in brake disc: An overview. *Dyna* **2021**, *88*, 23–31. [CrossRef]
19. Sivaranjani, S.; Velmurugan, S.; Kathiresan, K.; Karthik, M.; Gunapriya, B.; Gokul, C.; Suresh, M. Visualization of virtual environment through labVIEW platform. *Mater. Today Proc.* **2021**, *45*, 2306–2312. [CrossRef]
20. Martínez Bencardino, C. *Estadística Y Muestreo*; ECOE: Bogotá, Colombia, 2012.
21. Predictiva. Cálculo de los Parámetros de la Distribución de Weibul. WebPage. 2019. Available online: https://predictiva21.com/parametros-distribucion-weibull/ (accessed on 9 September 2024).
22. Gimenez Alvarez, J.M.; Gomez Targarona, J.C. Wind Generation Using Different Generatos Considering Their Impact on Power Systems. *Dyna* **2011**, *78*, 95–104. Available online: https://revistas.unal.edu.co/index.php/dyna/article/view/20070 (accessed on 12 May 2024).
23. Hemami, A. *Wind Turbine Technology*; Illustrate; Cengage Learning: Boston, MA, USA, 2012.
24. Kamoji, M.A.; Kedare, S.B.; Prabhu, S.V. Performance tests on helical Savonius rotors. *Renew. Energy* **2009**, *34*, 521–529. [CrossRef]
25. Uribe, I.M. Valuation of the wind as a source of wind energy in the state of Guerrero. *Ing.-Rev.* **2018**, *22*. Available online: http://www.nco.ncep.noaa.gov/pmb/products/ (accessed on 16 June 2024).
26. Samal, R.K. Assessment of wind energy potential using reanalysis data: A comparison with mast measurements. *J. Clean. Prod.* **2021**, *313*, 127933. [CrossRef]
27. Rahman, S.M.; Chattopadhyay, H. Statistical assessment of wind energy potential for power generation at Imphal, Manipur (India). *Energy Sources Part A Recovery Util. Environ. Eff.* **2023**, *45*, 7376–7388. [CrossRef]
28. Serrano Rico, J.C. Comparación de métodos para determinar los parámetros de Weibull para la generación de energía eólica. *Sci. Tech.* **2013**, *18*, 315–320. Available online: https://www.redalyc.org/articulo.oa?id=84929153004 (accessed on 13 June 2024).
29. Sánchez Hueto, L.J.L. *Diseño de un Generador Eólico Accionado por Corrientes Residuales Producidas por Automóviles*; Instituto Politecnico Nacional: Mexico City, Mexico, 2020.
30. Saad, M. Comparison of Horizontal Axis Wind Turbines and Vertical Axis Wind Turbines. *IOSR J. Eng.* **2014**, *4*, 27–30. [CrossRef]
31. Tong, W. *Wind Power Generation and Wind Turbine Design*; WIT Press: Billerica, MA, USA, 2010.


**Disclaimer/Publisher's Note:** The statements, opinions and data contained in all publications are solely those of the individual author(s) and contributor(s) and not of MDPI and/or the editor(s). MDPI and/or the editor(s) disclaim responsibility for any injury to people or property resulting from any ideas, methods, instructions or products referred to in the content.